Research Square

Preprints are preliminary reports that have not undergone peer review.
They should not be considered conclusive, used to inform clinical practice,
or referenced by the media as validated information.

A Meshless Collocation Framework for Free Vibration Analysis of Multilayer Functionally Graded Hyperelastic Beams with Experimental Validation and ANN Prediction

Qahtan A Jawad
University of Basrah
Haider Khazal
University of Basrah
Darya Ahmadova
Azerbaijan State Oil and Industry University
Deekshant Varshney
Chitkara University
Subhav Singh
Chitkara University
Narinderjit Singh Sawaran Singh
INTI International University
Omid Azarniya
a.omid@modares.ac.ir

Tarbiat Modares University

Research Article

Keywords: Hyperelastic Materials, Functionally Graded Materials, Neo-Hookean Strain-Energy Model, Meshless Collocation Method, Finite Element Method, Experimental Modal Analysis, Artificial Neural Networks

Posted Date: October 27th, 2026

DOI: https://doi.org/10.21203/rs.3.rs-11370616/v1

License: This work is licensed under a Creative Commons Attribution 4.0 International License.
Read Full License

Additional Declarations: No competing interests reported.

A Meshless Collocation Framework for Free Vibration Analysis of Multilayer Functionally Graded Hyperelastic Beams with Experimental Validation and ANN Prediction

Qahtan A. Jawad[1], Haider Khazal[1], Darya Ahmadova[2], Deekshant Varshney[3,4,5], Subhav Singh[3], Narinderjit Singh Sawaran Singh[6], Omid Azarniya[*].

[1] Department of Mechanical Engineering, College of Engineering, University of Basrah, Iraq; ORCID:
[2] Azerbaijan State Oil and Industry University, Baku, Azerbaijan; Research fields: Artificial Intelligence, Machine Learning, Data Science;
[3] Centre of Research Impact and Outcome, Chitkara University, Rajpura 140417, Punjab, India.
[4] Division of Research and Development, Lovely Professional University, Phagwara, Punjab, India.
[5] Center for Innovation and Inclusive Research, Sharda University, Greater Noida, Uttar Pradesh, India;
[6] Faculty of Data Science and Information Technology, INTI International University, Persiaran Perdana BBN, Putra Nilai, Negeri Sembilan, Malaysia;
[7]* Department of Mechanical Engineering, Tarbiat Modares University, Tehran, Iran;

Abstract

This research investigates the free vibration characteristics of hyperelastic functionally graded material (FGM) beams through an integrated numerical and experimental framework. The governing equations of the hyperelastic beam are formulated based on the Neo-Hookean strain-energy model in conjunction with Timoshenko beam theory and subsequently solved using the meshless collocation method (MCM). The reliability of the proposed numerical approach is assessed by comparison with experimental modal testing and finite element method (FEM) simulations. The investigation considers a square-cross-section rubber-based FGM beam composed of six different material compositions. The mechanical characteristics of the individual layers are experimentally evaluated through uniaxial tensile testing in accordance with the ASTM D412 standard. A detailed parametric investigation is then conducted to examine the effects of material parameters, geometric dimensions, and incompressibility coefficients on the dynamic response of the beam. The numerical findings obtained from the MCM show strong agreement with the FEM predictions. Furthermore, the discrepancy between the MCM results and the experimental modal measurements remains below 6.63%, demonstrating the validity of the proposed approach. Finally, a neural network (NN) model is incorporated as a complementary predictive tool to estimate the vibrational response of the investigated structure. The results confirm that the proposed neural network can effectively approximate the natural frequencies of the hyperelastic FGM beam with high accuracy.

Keywords: Hyperelastic Materials; Functionally Graded Materials; Neo-Hookean Strain-Energy Model; Meshless Collocation Method; Finite Element Method; Experimental Modal Analysis; Artificial Neural Networks.

*. Corresponding authors
Email Address: a.omid@modares.ac.ir

1.Introduction

Many engineering components are subjected to loading conditions that produce large deformations and finite strains, making the assumptions of classical linear elasticity inadequate. To accurately characterize the mechanical response under such conditions, nonlinear constitutive formulations are required. Among these, hyperelastic models have become a widely accepted framework for describing soft solids that undergo recoverable large deformations. Materials such as rubber, elastomeric foams, gels, and biological tissues exhibit this nonlinear elastic response and are commonly represented through strain energy density functions, which provide the basis for predicting their stress–strain relationship and structural performance under finite deformation. The nonlinear dynamics of hyperelastic and functionally graded structures have received considerable attention in recent years. In this context, Shakeriaski and Ghodrat[1] examined thermo-hyperelastic wave propagation in near-incompressible FGM media under combined mechanical and thermal loading, demonstrating the role of material gradation in modifying wave characteristics. Related studies have extended the analysis to structural components, including hyperelastic beams [2, 3], cylindrical shells[4], membranes [5], and rotating disks with variable thickness [6, 7]. These investigations have generally emphasized the effects of material nonlinearity, geometric parameters, and boundary or foundation conditions on the resulting dynamic response. In parallel, the behavior of FGM structures has been examined under Multiphysics and advanced material conditions, such as thermo-hyperelastic coupling [8], piezo-viscoelastic effects [9], and flexoelectricity and porosity in microstructures [10]. Despite these developments, the existing literature has primarily relied on analytical and numerical formulations, while experimental characterization of the free-vibration response of multilayer hyperelastic FGM beams remains relatively limited. Moreover, the combined use of experimental modal testing, meshless numerical techniques, finite element simulations, and neural-network-based prediction has received comparatively little attention. These aspects motivate the present study, which investigates the free vibration of a multilayer hyperelastic FGM beam through numerical analysis, experimental validation, and neural-network prediction.
Karmi Mohammadi [11] developed an improved Biederman model for microbeam structures. Based on the modified couple stress theory, the proposed model was employed to account for size-dependent and nonlinear material effects. The governing equations of microbeam motion were derived using Hamilton's principle and solved through discretization and the Galerkin perturbation method. Khaniki et al. [12, 13] investigated the nonlinear vibrations and mechanical behavior of nonlinear elastic systems undergoing axial motion. They also examined the bending response and internal resonance of thick visco-hyperelastic arches subjected to time-dependent external loads. Azarniya and Rahimi[14] numerically and experimentally studied the vibration characteristics and static deflection of sandwich structures incorporating a nonlinear elastic core. Zolfagharian et al. [15] investigated the low-frequency vibration characteristics and global buckling behavior of hyperelastic cylindrical tubes through a combination of experimental and numerical approaches.

In recent years, meshless numerical methods have gained significant attention as effective tools for solving nonlinear problems involving large deformations. Among these approaches, the Meshless Collocation Method (MCM) has emerged as an efficient and accurate technique for the analysis of hyperelastic structures. Unlike the conventional finite element method, MCM discretizes the computational domain using scattered nodes without requiring predefined elements or a background mesh. This mesh-independent formulation eliminates mesh distortion during large deformations, making the method particularly suitable for geometrically nonlinear analyses while maintaining computational efficiency.Chen and Ling [16] developed an extrinsic meshless

collocation method for solving partial differential equations defined on manifolds. Zhang et al.[17] proposed a localized meshless collocation method incorporating a partial upwind scheme for convection-dominated diffusion problems. Hosseini et al.[18] employed a radial-basis-function-based meshless collocation method to investigate the free and forced vibrations of functionally graded plates based on first-order shear deformation theory. Li et al. [19] developed an efficient localized meshless collocation method for solving two-dimensional Burgers-type equations arising in turbulent fluid flows. Zhang[20] introduced a meshless symplectic and multi-symplectic local radial basis function collocation method for Hamiltonian partial differential equations. Abbaszadeh and Pourbashash et al. [21] proposed a local meshless collocation method for solving two-dimensional fractional Klein–Kramers equations on irregular domains. Patel and Rachchh[22] reviewed recent developments in meshless methods and discussed their applications in various engineering and computational problems. Radmanesh and Ebadi[23] presented a local meshless collocation method for solving time-dependent fractional integral equations and demonstrated its computational efficiency compared with conventional global approaches.

Nowadays, artificial neural networks (ANNs) have become widely used for predicting the response of complex engineering structures due to their ability to capture nonlinear relationships between input parameters and structural behavior. Trained using numerical or experimental data, ANN models can accurately estimate dynamic characteristics, such as natural frequencies and mode shapes, with substantially lower computational cost than conventional numerical simulations. Consequently, ANN-based approaches have become valuable tools for rapid prediction, parametric analysis, and structural optimization of nonlinear systems. Siłka et al.[24] developed a recurrent neural network (RNN) model based on long short-term memory (LSTM) architecture to predict vibrations of high-speed trains from time-series data. Fissha et al. [25] applied a Bayesian neural network (BNN) to predict blast-induced ground vibrations and evaluated its capability for estimating vibration velocity. Lawal and Idris[26, 27] developed an artificial neural network (ANN)-based mathematical model for predicting blast-induced ground vibrations using available data from the literature. Liang et al.[28] proposed a Bayesian neural network approach for predicting train-induced ground vibrations while accounting for uncertainty in the predictions. Zollanvari et al.[29] employed a deep recurrent neural network to analyze vibration signals and predict transformer faults under different excitation conditions. Shang et al.[30] combined the firefly optimization algorithm with an artificial neural network to predict blast-induced ground vibrations in open-pit mines. Tang et al. [31] developed a transfer-learning physics-informed neural network (TL-PINN) for vortex-induced vibration prediction, reducing the dependence of neural networks on large training datasets. Lawal [27] proposed an ANN-based model for predicting blast-induced ground vibrations in granite quarries and demonstrated its applicability as an alternative to conventional prediction approaches. Jamil et al. [32]developed a neural-network-based predictive controller for vibration suppression in tall structures and experimentally evaluated its performance. Nguyen and Bui [33] proposed a hunger games search optimization-based artificial neural network for predicting blast-induced ground vibration intensity and investigated the effect of network topology on prediction accuracy.

The present study investigates the free vibration behavior of functionally graded hyperelastic (FGH) beams with a square cross-section composed of multiple natural rubber layers exhibiting gradually varying material properties. The nonlinear constitutive behavior is described using the Neo-Hookean strain energy function, while Timoshenko beam theory is adopted to account for both bending and shear deformations. The governing equations are solved using the Meshless Collocation Method (MCM) based on radial basis function interpolation and validated through finite element simulations in Abaqus as well as experimental modal testing. Furthermore, an artificial neural network (ANN) is developed to establish the relationship between the beam

geometry, material parameters, and the corresponding natural frequencies. The proposed ANN enables rapid and accurate prediction of the dynamic response, providing a computationally efficient alternative to repeated numerical analyses for parametric investigations and preliminary structural design of FGH beams.

2. Constitutive relations

A six-layer functionally graded hyperelastic (FGH) beam is considered to examine its free vibration characteristics. The beam has a square cross-section measuring (20 ×20) mm and a reference length of (L = 250) mm, as depicted in Figure. 1. To achieve a gradual variation in mechanical properties, the beam thickness is divided into six equal sublayers, each with a thickness of 3.33 mm. Different values of the Neo-Hookean material constant (C_{10}) are assigned to each layer, producing a continuous stiffness gradient across the thickness. The interfaces between adjacent layers are assumed to be perfectly bonded, ensuring full displacement compatibility and preventing any interfacial separation during vibration. A Cartesian coordinate system is introduced to describe the beam geometry, where the longitudinal direction coincides with the (x)-axis, the width is aligned with the (y)-axis, and the thickness is measured along the (z)-axis. Throughout the analysis, both beam ends are fully constrained, corresponding to a clamped–clamped boundary condition employed in the numerical and experimental investigations.

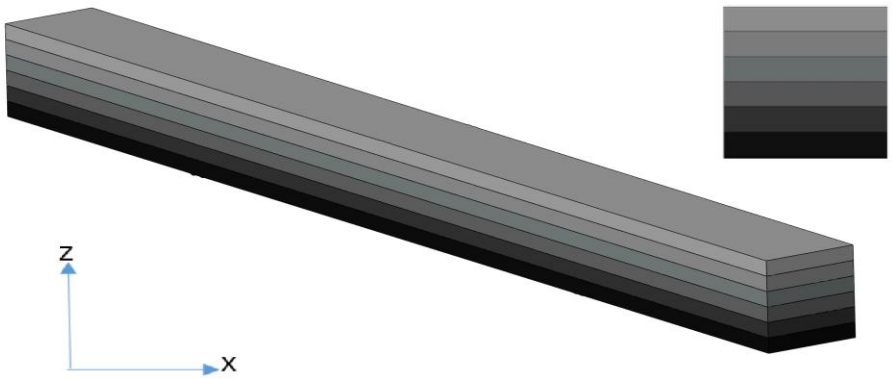


Figure 1. Six-layer functionally graded hyperelastic beam.

According to Timoshenko beam theory, the displacement field is defined as:

$$w(x,z,t) = w(x,t)$$
$$u(x,z,t) = u(x,t) + z\varphi(x,t) \quad (1)$$

In the above expressions, (u (x, t)) and (w (x, t)) correspond to the axial and transverse displacements of the beam centroidal axis, respectively, whereas ($\varphi(x,t)$) denotes the rotation of the beam cross-section about the (y)-axis. Owing to the large strains and finite deformations associated with hyperelastic materials, geometric nonlinearities must be incorporated into the formulation. Therefore, the Green–Lagrange strain tensor is employed, and the corresponding nonlinear strain–displacement relationships are obtained as follows:

$$\varepsilon_{xx} = \frac{\partial u}{\partial x} = \frac{z\partial\varphi}{\partial x} + \frac{1}{2}\left(\frac{\partial w}{\partial x}\right)^2$$
$$\varepsilon_{xz} = \frac{\partial u}{\partial z} + \frac{\partial w}{\partial x} = \varphi + \frac{\partial w}{\partial x} \quad (2)$$

The quadratic term represents the geometric nonlinearity arising from finite rotations and large transverse deflections. To accurately describe the resulting deformation, the kinematics of the beam are formulated using the right Cauchy–Green deformation tensor, which provides an appropriate strain measure for hyperelastic materials undergoing large deformations. The tensor is expressed as:

$$C = 2E + I = \begin{bmatrix} 2\varepsilon_{xx} + 1 & \varepsilon_{xy} & \varepsilon_{xz} \\ \varepsilon_{xy} & 1 & \varepsilon_{yz} \\ \varepsilon_{xz} & \varepsilon_{yz} & 2\varepsilon_{zz} + 1 \end{bmatrix} \quad (3)$$

In this expression, (F) represents the deformation gradient tensor, which maps the material configuration from the undeformed state to the current deformed configuration. Based on the right Cauchy–Green deformation tensor, the first and third invariants are defined, respectively, as

$$I_1 = trace(C) = 2(\varepsilon_{xx} + \varepsilon_{zz}) + 3$$
$$I_3 = det(C) = -{\varepsilon_{xz}}^2 + 2\varepsilon_{zz} + 2\varepsilon_{xx} + 4\varepsilon_{xx}\varepsilon_{zz} + 1 \quad (4)$$

The hyperelastic beam is assumed to be composed of an incompressible material. By enforcing the incompressibility constraint, the normal strain in the (z)-direction can be determined from Eq. (5). This relationship ensures that the volumetric deformation remains unchanged throughout the loading process and is expressed as [43],

$$I_3 = 1 \rightarrow \varepsilon_{zz} = -\frac{1}{2}\left(\frac{2\varepsilon_{xx} - \varepsilon_{xz}^2}{2\varepsilon_{xx} - \varepsilon_{xy}^2 + 1}\right) \quad (5)$$

Therefore, based on the Taylor expansion, ε_{zz} is calculated as follows [44].

$$\varepsilon_{zz} = -4{\varepsilon_{xx}}^3 + 2{\varepsilon_{xx}}^2 - \varepsilon_{xx}{\varepsilon_{xz}}^2 - \varepsilon_{xx} + \frac{{\varepsilon_{xz}}^2}{2} \quad (6)$$

The constitutive response of the graded beam is represented using the Neo-Hookean strain-energy density function. To account for the functional gradation, each layer is assigned a distinct Neo-Hookean material constant, ($C_{10}^{(i)}$), determined from the corresponding uniaxial tensile experiments. Consequently, the strain-energy density function for the (i) layer can be written as,

$$w^{(i)} = \int C_{10}^{(i)}(I_1 - 3) = 2C_{10}^{(i)}(\varepsilon_{xx} + \varepsilon_{zz}) \quad i = 1,2, \dots \dots, 6. \quad (7)$$

By substituting Eq. (6) in Eq. (7), the neo-Hookean strain energy function for the Timoshenko beam is obtained as:

$$w^{(i)} = \int C_{10}^{(i)}(I_1 - 3) = 2C_{10}^{(i)}(-8{\varepsilon_{xx}}^3 + 4{\varepsilon_{xx}}^2 - 2\varepsilon_{xx}{\varepsilon_{xz}}^2 + {\varepsilon_{xz}}^2) \ ,$$
$$i = 1,2, \dots \dots, 6. \quad (8)$$

where the strain-energy function is evaluated independently for each hyperelastic layer according to its corresponding Neo-Hookean material constant. A beam's kinetic energy (K) can be calculated as follows:

$$K = \frac{1}{2}\int \rho\,(\dot{u}^2 + \dot{w}^2)\,dV \quad (9)$$

The total potential energy of the functionally graded hyperelastic beam is therefore expressed as; where i denotes the domain occupied by the i-th hyperelastic layer.

$$\Pi = w^{(i)} + K$$
$$= \int 2C_{10}^{(i)}(-8\varepsilon_{xx}^3 + 4\varepsilon_{xx}^2 - 2\varepsilon_{xx}\varepsilon_{xz}^2 + \varepsilon_{xz}^2) \; + \frac{1}{2}\int \rho\,(\dot{u}^2 + \dot{w}^2)\,dV \quad ,$$
$$i = 1,2,\ldots\ldots,6. \tag{10}$$

3. Nonlinear Governing Equations of the Functionally Graded Hyperelastic Beam

The nonlinear equilibrium equations governing the proposed functionally graded hyperelastic (FGH) beam are derived using the principle of stationary total potential energy. By applying the Euler–Lagrange equations to the total potential energy functional, the governing equations of the multilayer beam are obtained as follows: [45].

$$\frac{\partial \Pi}{\partial S} - \frac{\partial}{\partial x}\left(\frac{\partial \Pi}{\partial S_{,x}}\right) = 0, S = w, \varphi_x, u \tag{12}$$

where u(x), w(x), and ϕ(x) denote the axial displacement, transverse displacement, and rotation of the beam cross-section, respectively. The corresponding essential and natural boundary conditions are given by;

$$S = 0 or \left(\frac{\partial \Pi}{\partial S_{,x}}\right)n_x + \left(\frac{\partial \Pi}{\partial S_{,y}}\right)n_y = 0 S = w, \varphi_x, u \tag{13}$$

where nx and ny denote the components of the outward unit normal vector on the beam boundary. By substituting the constitutive relations presented in Section 2 into Eq. (12), three coupled nonlinear differential equations governing the static response of the multilayer functionally graded hyperelastic (FGH) beam are obtained. The governing equations corresponding to the virtual variations δu, δw, and δϕ are expressed as follows:

$$\delta u: 24A\left(\frac{d}{dx}w(x)\right)^3\frac{d^2}{dx^2}w(x) + 24A\left(\frac{d^2}{dx^2}u(x)\right)\left(\frac{d}{dx}w(x)\right)^2$$
$$- 2\left(-24A\frac{d}{dx}u(x) + 2A\right)\left(\frac{d}{dx}w(x)\right)\frac{d^2}{dx^2}w(x)$$
$$+4A\varphi(x)\frac{d^2}{dx^2}w(x) + 48A\left(\frac{d}{dx}u(x)\right)\frac{d^2}{dx^2}u(x) + 4A\varphi(x)\frac{d}{dx}\varphi(x) + 48D\left(\frac{d}{dx}\varphi(x)\right)\frac{d^2}{dx^2}\varphi(x)$$
$$= I_0\ddot{u}_0$$
$$\delta w: 30A\left(\frac{d}{dx}w(x)\right)^4\frac{d^2}{dx^2}w(x) + 24A\left(\frac{d^2}{dx^2}u(x)\right)\left(\frac{d}{dx}w(x)\right)^3$$
$$+ 72A\left(\frac{d}{dx}u(x)\right)\left(\frac{d}{dx}w(x)\right)^2\frac{d^2}{dx^2}w(x) + 6A\left(\frac{d}{dx}\varphi(x)\right)\left(\frac{d}{dx}w(x)\right)^2$$
$$+ 12A\varphi(x)\left(\frac{d}{dx}w(x)\right)\frac{d^2}{dx^2}w(x) + 4A\left(\frac{d}{dx}\varphi(x)\right)\left(\frac{d}{dx}u(x) - 1/2\right)$$
$$- 2\left(-2A\varphi(x)\frac{d}{dx}\varphi(x) - 24A\left(\frac{d}{dx}u(x)\right)\frac{d^2}{dx^2}u(x) - 24D\left(\frac{d}{dx}\varphi(x)\right)\frac{d^2}{dx^2}\varphi(x)\right.$$
$$\left. + 2A\frac{d^2}{dx^2}u(x)\right)\frac{d}{dx}w(x) - 12D\left(\frac{d}{dx}\varphi(x)\right)^2 + 4A\varphi(x)\frac{d^2}{dx^2}u(x)$$
$$- 2\left(-A(\varphi(x))^2 - 12A\left(\frac{d}{dx}u(x)\right)^2 + 2A\frac{d}{dx}u(x) + A\right)\frac{d^2}{dx^2}w(x) = I\ddot{\varphi} \tag{14}$$

$$\delta\varphi = -2A\left(\frac{d}{dx}w(x)\right)^3 - 2A\varphi(x)\left(\frac{d}{dx}w(x)\right)^2 - 4A\left(\frac{d}{dx}u(x) - 1/2\right)\frac{d}{dx}w(x) - 4A\varphi(x)\frac{d}{dx}u(x)$$
$$+2\varphi(x)A + 24D\left(\frac{d^2}{dx^2}\varphi(x)\right)\left(\frac{d}{dx}w(x)\right)^2 + 48D\left(\frac{d}{dx}\varphi(x)\right)\left(\frac{d}{dx}w(x)\right)\frac{d^2}{dx^2}w(x)$$
$$+48D\left(\frac{d^2}{dx^2}\varphi(x)\right)\frac{d}{dx}u(x) + 48D\left(\frac{d}{dx}\varphi(x)\right)\frac{d^2}{dx^2}u(x) - 8D\frac{d^2}{dx^2}\varphi(x) = I_0\ddot{w}$$

Their explicit forms are identical to those derived for the homogeneous hyperelastic FGM beam, with the exception that the stiffness coefficients are evaluated using the functionally graded material properties. Likewise, substituting Eq. (11) into Eq. (13) yields the corresponding natural boundary conditions for the functionally graded hyperelastic (FGH) beam, which are given by:

$$[6A(\frac{d\omega(x)}{dx})^4 - 4A\varphi(x)(\frac{d\omega(x)}{dx}) + (-24A(\frac{du(x)}{dx}) + 2A)(\frac{d\omega(x)}{dx})^2 - 2A\varphi(x)^2 - 24D(\frac{d\varphi(x)}{dx})^2$$
$$+4A(\frac{du(x)}{dx}) - 24(\frac{du(x)}{dx})^2]n_x[-2A\varphi(x)(\frac{d\omega(x)}{dx})]n_y = 0 or u = 0$$

$$[-6A(\frac{d\omega(x)}{dx})^5 - 24A(\frac{du(x)}{dx})(\frac{d\omega(x)}{dx})^3 - 6A\varphi(x)(\frac{d\omega(x)}{dx})^2 - 24A(\frac{du(x)}{dx})^2 + 4A\frac{du(x)}{dx}$$
$$- 24D(\frac{d\varphi(x)}{dx})^2 + 2A(\frac{d\omega(x)}{dx}) - 4A\frac{d\varphi(x)}{dx}\frac{du(x)}{dx} - 2A\varphi^2(x)$$
$$-1/2\varphi(x)]n_x[-6A(\frac{d\omega(x)}{dx})^4 - 16A(\frac{du(x)}{dx})(\frac{d\omega(x)}{dx})^3 \quad (15)$$
$$-4A(\frac{d\omega(x)}{dx})\varphi(x) - 8A(\frac{du(x)}{dx})^2 - 8D(\frac{d\varphi(x)}{dx})^2]n_y = 0 or w = 0$$
$$[-8D((3\frac{d\omega(x)}{dx})^2 + 6(\frac{du(x)}{dx}) - 1)(\frac{d\varphi(x)}{dx})^2]n_x = 0 or \varphi(x) = 0$$

Unlike the homogeneous beam formulation, the generalized extensional and bending stiffness coefficients are evaluated by assembling the contribution of each hyperelastic layer,

$$A = \sum_{i=1}^{8} A_{i=} \int_{z_{i-1}}^{z_i} C_{10}^{(i)} dz$$
$$D = \sum_{i=1}^{8} D_{i=} \int_{z_{i-1}}^{z_i} C_{10}^{(i)} z^2 dz$$
$$I_0 = \rho h I = \frac{1}{12}\rho h^3 \quad (16)$$

4. Numerical analysis

The free vibration behavior of the proposed functionally graded hyperelastic (FGH) beam is investigated using the Meshless Collocation Method (MCM) and validated through finite element (FE) simulations and experimental measurements. The FE model is developed in ABAQUS, whereas the meshless numerical formulation is implemented in MATLAB. The accuracy and reliability of the proposed computational framework are assessed through comparisons between the numerical predictions and the experimental results. The FGH beam consists of six perfectly bonded hyperelastic layers, each characterized by a distinct Neo–Hookean material parameter, thereby producing a continuous through-thickness stiffness gradient.

4.1 meshless collocation method

The nonlinear governing equations of the functionally graded hyperelastic (FGH) beam are solved using the Meshless Collocation Method (MCM). Unlike conventional element-based numerical methods, the proposed approach relies solely on a set of discrete collocation points distributed throughout the computational domain, thereby eliminating the need for mesh generation and element connectivity. This mesh-independent formulation is particularly advantageous for the analysis of hyperelastic structures undergoing large deformations and strong geometric nonlinearities. As illustrated in Fig. 2, the computational domain is discretized into two categories of nodes: interior collocation points and boundary nodes. The governing differential equations are enforced at the interior collocation points, whereas the essential and natural boundary conditions are imposed at the boundary nodes. This nodal discretization enables the MCM to accurately capture the nonlinear structural response while maintaining a simple, efficient, and robust numerical implementation.

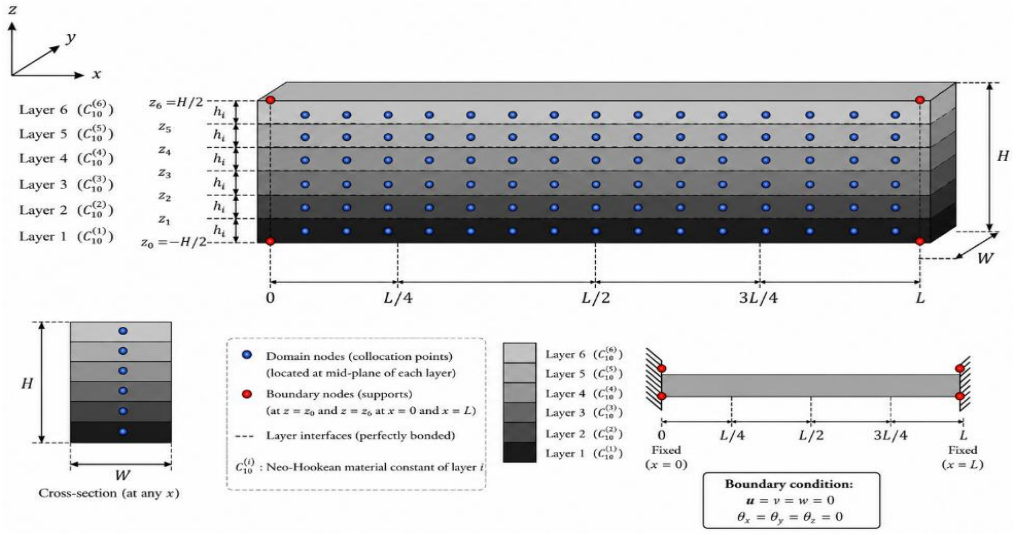


Figure 2. Boundary and interior collocation nodes in the MCM.

Accordingly, the governing equations of the functionally graded hyperelastic (FGH) beam can be written in the following general operator form:

$$Lu = f in \Omega,$$

subject to the boundary conditions, (17)

$$L_B u = g on \partial\Omega$$

where L denotes the differential operator governing the field equations, f is the body force vector, u represents the vector of field variables, g is the prescribed boundary data, and LB denotes the boundary differential operator associated with the derivative (natural) boundary conditions. The field variables are approximated using multiquadric radial basis functions (MQ-RBFs), as expressed in Eq. (18).

$$\begin{Bmatrix} w \\ \varphi_x \\ u \end{Bmatrix} = \sum_{i=1}^{N} \phi_i \begin{Bmatrix} a_i^w \\ a_i^{\varphi_x} \\ a_i^u \end{Bmatrix} \tag{18}$$

Where N is the total number of nodes, and a is the unknown vector in the domain of beam. φ_i Are the radial basis function (RBF) which are defined as relations (19 and 20).[46]

$$\phi = [R^T(x)S_a + p^T(x)S_b] \tag{19}$$

and

$$R^T(x) = [R_1(x), R_2(x), \dots, R_n(x)]$$
$$p^T(x) = [p_1(x), p_2(x), \dots, p_m(x)]$$
$$S_b = \left[P_m^T R_Q^{-1} P_m\right]^{-1} P_m^T R_Q^{-1}$$
$$S_a = R_Q^{-1}[1 - P_m S_b]$$
$$R_Q = \begin{bmatrix} R_1(x_1) & R_2(x_1) & \cdots & R_n(x_1) \\ R_1(x_2) & R_2(x_2) & \cdots & R_n(x_2) \\ \vdots & \vdots & \ddots & \vdots \\ R_1(x_n) & R_2(x_n) & \cdots & R_n(x_n) \end{bmatrix}$$
$$P_m = \begin{bmatrix} P_1(x_1) & P_2(x_1) & \cdots & P_m(x_1) \\ P_1(x_2) & P_2(x_2) & \cdots & P_m(x_2) \\ \vdots & \vdots & \ddots & \vdots \\ P_1(x_n) & P_2(x_n) & \cdots & P_m(x_n) \end{bmatrix}$$
$$p^T = [1, x, x^2, \dots] \tag{20}$$

This paper investigates the thin-plate spline basis function (TPS).

$$R_i(x) = ((x - x_i)^2)^{\frac{\eta}{2}} \tag{21}$$

η in Eq. (21) is the shape parameter of the RBF. Unlike the homogeneous hyperelastic beam investigated in the previous study, the present beam consists of six functionally graded hyperelastic layers. Therefore, the Neo-Hookean material parameter varies through the beam thickness according to $C_{10} = (z)$, which is represented numerically by six discrete values,

$$C_{10}(1), C_{10}(2) \ , \cdots, C_{10}(6)$$

The nonlinear differential equations are obtained by substituting Eq. (18) in Eqs. (15 and 14). Consequently, the matrix form of the governing equations is obtained.

$$[K_L + K_{NL}(a)]\{a\} + M\{\ddot{a}\} = 0 \tag{22}$$

where K_L and K_{NL} denote the linear and nonlinear stiffness matrices, respectively, a is the nodal variable vector, and M is the mass matrix.

$$K_{L,NL}(a) = \begin{bmatrix} \frac{\partial \delta w}{\partial W} & \frac{\partial \delta w}{\partial \varphi^x} & \frac{\partial \delta w}{\partial u} \\ \frac{\partial \delta \varphi_x}{\partial W} & \frac{\partial \delta \varphi_x}{\partial \varphi^x} & \frac{\partial \delta \varphi_x}{\partial u} \\ \frac{\partial \delta u}{\partial W} & \frac{\partial \delta u}{\partial \varphi^x} & \frac{\partial \delta u}{\partial u} \end{bmatrix} \tag{23}$$

Due to the presence of both geometric and material nonlinearities in the governing equations, an incremental–iterative solution strategy is employed. In this study, the nonlinear equilibrium equations are solved using the arc-length continuation method, which provides a stable approach for tracking the complete nonlinear equilibrium path, especially in the vicinity of critical points and limit points. The nonlinear analysis begins with the linear solution, which is used as the initial approximation for the subsequent iterative procedure. The nonlinear response is then obtained through a series of incremental load steps, where the converged solution from each increment serves as the initial guess for the following step. The iterative procedure is continued until the relative difference between two consecutive iterations is reduced below 0.1%, indicating satisfactory convergence of the numerical solution.

The complete computational framework and solution algorithm of the Meshless Collocation Method (MCM) are presented in Figure 3.

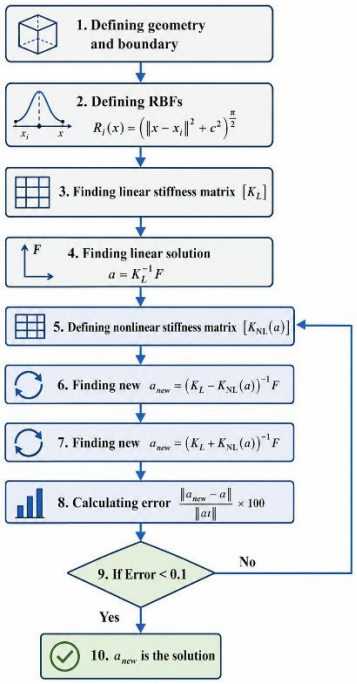


Figure 3. Flowchart of the proposed solution procedure for the nonlinear FGH beam.

3.2. Finite element method

The finite element (FE) model of the functionally graded hyperelastic (FGH) beam was established in Abaqus/Standard, as shown in Figure 4. A mesh convergence analysis was first performed to ensure sufficient numerical accuracy, and an element size of 1 mm was selected for the final simulations. The developed model contained 128,541 nodes and 90,060 C3D8RH hybrid hexahedral elements, which are particularly suitable for representing the nearly incompressible behavior of hyperelastic materials. The beam was modeled as a six-layer structure with a gradual variation of the Neo-Hookean material parameter C_{10} across the thickness direction to describe the functionally graded configuration. Geometric nonlinearity was considered during the analysis, and the constitutive behavior of each layer was defined using the Neo-Hookean hyperelastic formulation. To replicate the experimental free vibration conditions, both beam ends were fully constrained by restricting all translational and rotational degrees of freedom (Figure 5). The natural frequencies and corresponding mode shapes were subsequently obtained using the Lanczos eigenvalue extraction method.

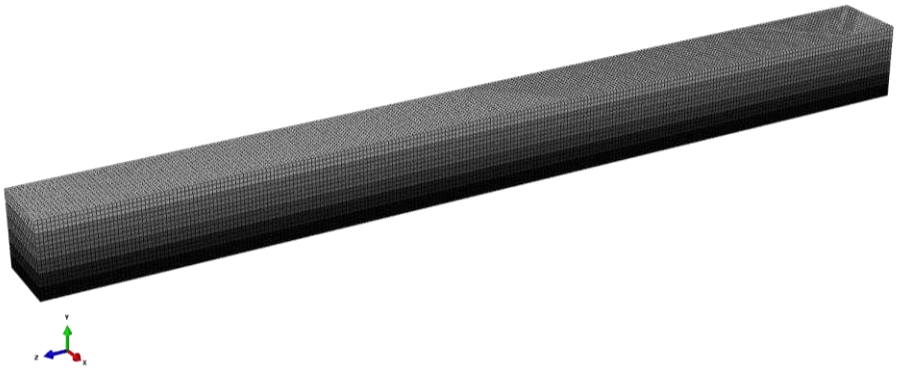


Figure 4. Free vibration Finite element of FGM beam.

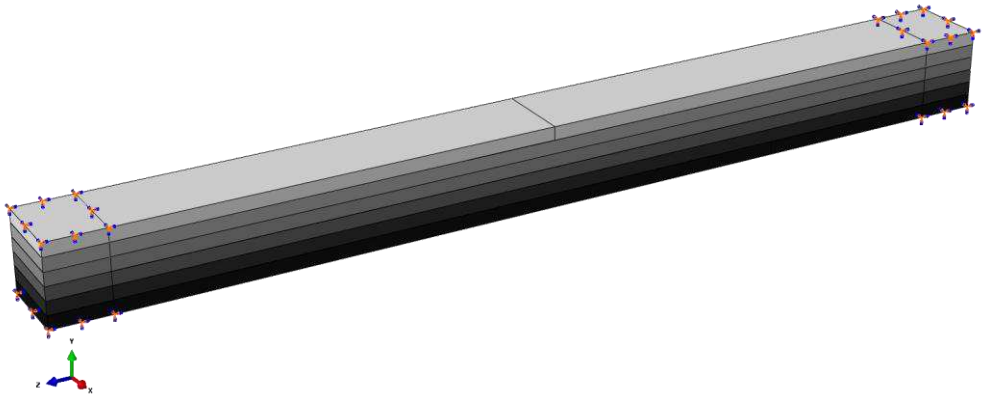


Figure 5. Free vibration Finite element of FGM beam.

5. Materials and experimental procedures of FGM beam

5.1. Fabrication of Rubber FGM Beams

To experimentally validate the developed numerical framework, six natural rubber formulations were manufactured based on the compositions presented in Table 1 and subsequently employed to produce the functionally graded hyperelastic (FGH) beam. The variation in mechanical properties across the beam thickness was achieved by assigning a distinct rubber formulation to each individual layer. The fabrication process was based on conventional rubber vulcanization, in which the raw elastomer is transformed into a stable hyperelastic structure through the incorporation of reinforcing agents, sulfur, activators, accelerators, and other chemical additives. During vulcanization, the formation of cross-links between polymer chains enhances the mechanical strength, stiffness, and elastic recovery capability of the rubber network. The rubber formulations were initially homogenized using a laboratory two-roll mill operating at 40 rpm for approximately 10 min to achieve uniform dispersion of the constituents. Subsequently, the pre-mixed ingredients were transferred to a Banbury internal mixer, where Standard Malaysian Rubber (SMR), polybutadiene rubber (PBR), and carbon black (N660) were incorporated and blended for approximately 5 min. The remaining additives, including TBBS accelerator, zinc oxide, stearic acid, sulfur, and other constituents listed in Table 1, were then added gradually and mixed for an additional 5–7 min to complete the compounding procedure and promote uniform distribution of the vulcanization agents. After mixing, the resulting rubber compounds were processed through the two-roll mill to obtain sheets with controlled thickness and consistent quality. These individual rubber sheets were subsequently used as separate graded layers for assembling the functionally graded hyperelastic beam, as illustrated in Figure 6.

Ingredients\ Compound(gram)	1	2	3	4	5	6
(PBR-1220) Butadiene rubber	480	590	790	890	990	1090
(SMR-20) Natural rubber	587	510	410	310	210	110
(N660) Carbon Black	533	500	400	300	200	100
Spindle oil	74	74	74	74	74	74
Sulfur	21	21	21	21	21	21
TBBS	9	9	9	9	9	9
Antioxidants	16	16	16	16	16	16
ZnO	16	16	16	16	16	16
Stearic acid	16	16	16	16	16	16

Table 1. Formulation of the natural rubber compounds used for fabrication of the functionally graded hyperelastic beam.

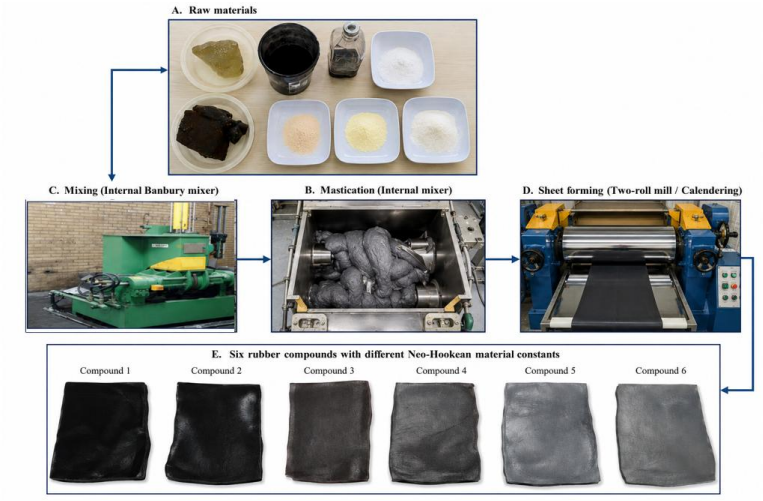


Figure 6. Fabrication procedure of the functionally graded hyperelastic (FGH) beam.

The curing characteristics of the developed rubber formulations were evaluated using a moving-die rheometer (MDR), as illustrated in Figure. 7. The MDR system consists of two enclosed dies with an oscillating rotor positioned between them, enabling real-time monitoring of the vulcanization reaction. Approximately 200 g of each rubber formulation was placed inside the test chamber and subjected to a constant temperature of 140 °C. During the measurement, the rotor oscillated at an angular displacement of ±1° under an applied torque of 20 lbf. As the vulcanization reaction proceeded, the formation of sulfur-based cross-links within the polymer chains progressively increased the stiffness of the rubber network, resulting in a continuous increase in the measured torque. The curing reaction was considered complete when the torque response reached a stable plateau, representing the optimum curing condition for specimen fabrication. For the investigated formulation, the maximum torque reached 63 lbf, and the stabilization of the curing curve occurred after approximately 10.2 min. These obtained curing parameters were subsequently applied during the fabrication of the FGH beam specimens to ensure consistent material properties and repeatable manufacturing conditions.



Figure 7. Moving-die rheometer setup for rubber curing characterization.

Figure 8 illustrates the fabrication procedure of the functionally graded hyperelastic (FGH) beam. A steel mold was initially designed in SolidWorks and fabricated from AISI MO40 steel using CNC machining to withstand the thermal and mechanical conditions during the vulcanization

process. Before molding, the rubber formulations were cut into small pieces and uniformly arranged inside the mold cavity to promote proper filling, reduce processing time, and prevent air void formation. The mold was then placed in a hot press and cured at 90 °C under a pressure of 0.5 MPa for 10.2 min, based on the optimum curing time obtained from the moving-die rheometer measurements. Each rubber formulation was manufactured individually to obtain six hyperelastic layers with different Neo-Hookean material characteristics. The produced layers were subsequently stacked according to the designed gradation profile and bonded using a cohesive adhesive at the interfaces to form the FGH configuration. Finally, the assembled beam underwent post-curing at 100 °C under a pressure of 2 bar to enhance interfacial bonding and ensure the structural integrity of the multilayer specimen. The fabricated FGH beam was then employed for the experimental and numerical investigations.

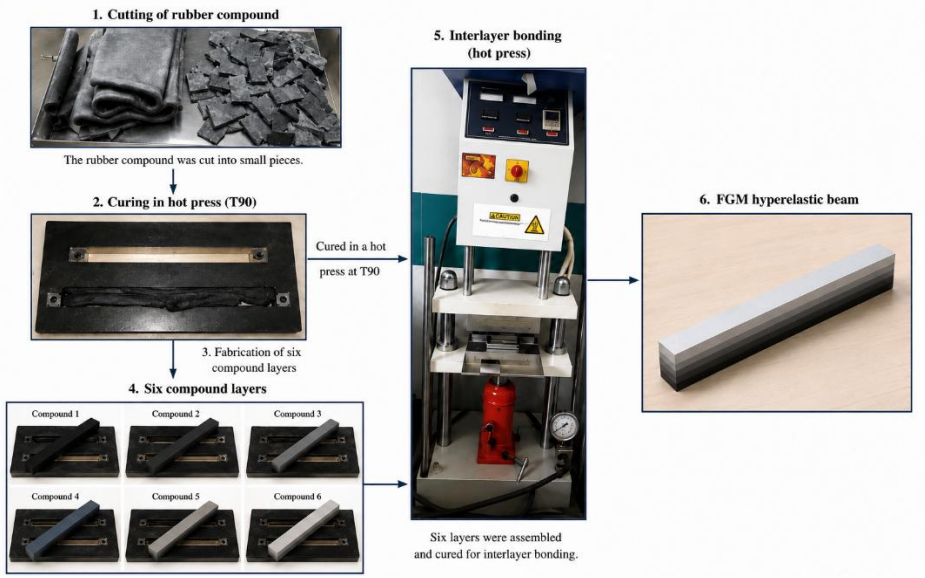


Figure 8. Identification of the Neo-Hookean material parameter from experimental tensile test data.

5.2. Mechanical properties of compounds

To characterize the mechanical properties of the six rubber compounds, uniaxial tensile tests were conducted at a crosshead speed of 10 mm/min and under ambient temperature conditions, in accordance with the ASTM D412 standard (Figure 9). As shown in Figure. 10, the experimental tensile test results were used to calibrate the Neo-Hookean strain energy function. Accordingly, the corresponding Neo-Hookean material coefficient was determined for each compound, as summarized in Table 2.

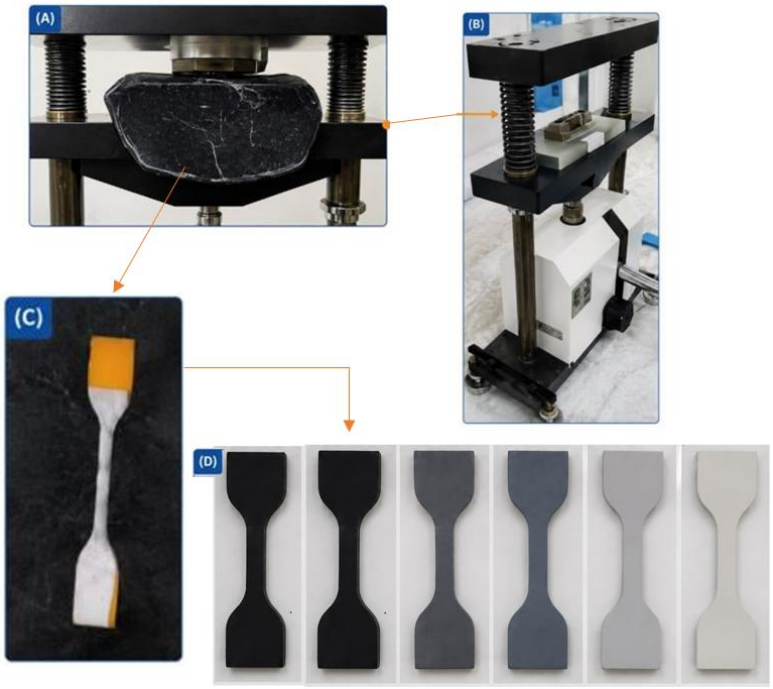


Figure 9. Fabrication of ASTM D412 specimens for six rubber compounds.

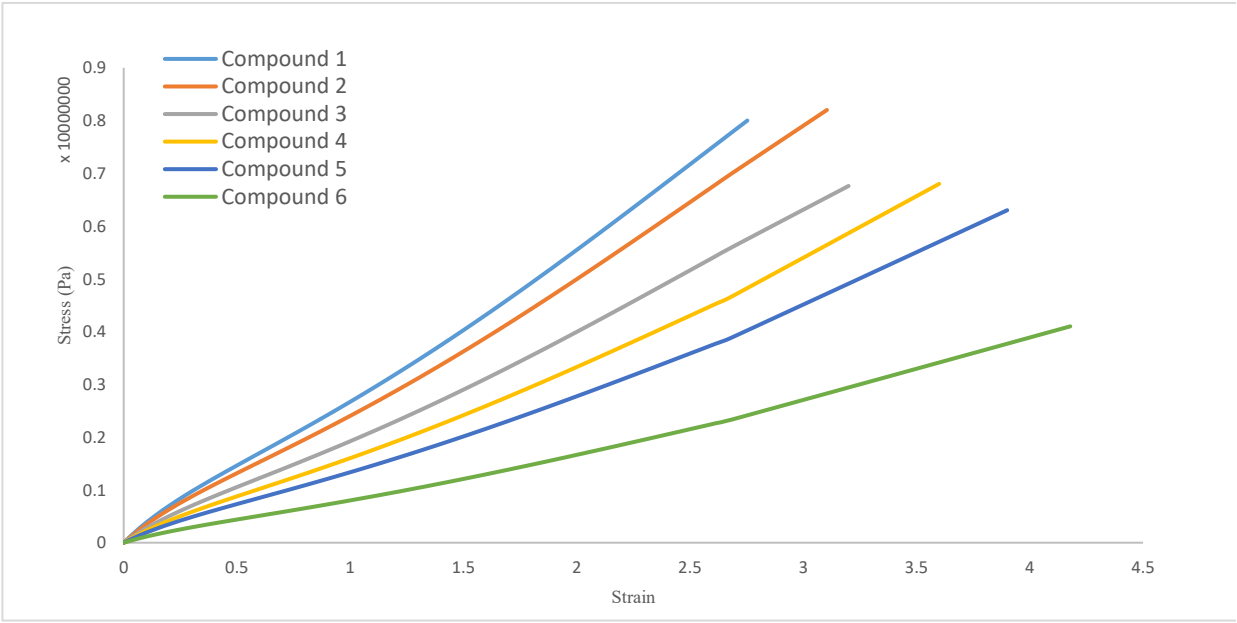


Figure 10. Stress-Starin displacement curves of six rubber compounds under ASTM D412 tensile testing.

Function \ Compound (Pa)	1	2	3	4	5	6
Neo-Hookean (C_{10})	307843.4	277059.06	246274.72	215490.38	200098.21	184706.04

Table 2. Neo-Hookean model fitting for six rubber compounds.

4.3. Experimental modal test

The dynamic response of the fabricated FGH beam was characterized experimentally using modal testing to determine its natural frequencies and corresponding mode shapes. The experimental arrangement included a rigid support fixture, an instrumented impact hammer, and an accelerometer for excitation and response acquisition (Figure 11). During testing, the beam was mounted between a high-stiffness support base and a metal plate secured by four screws to provide stable and repeatable boundary conditions. A two-channel data acquisition system was used, with one channel measuring the excitation force from the impact hammer and the other recording the acceleration response of the beam. Each measurement was repeated five times to improve accuracy and ensure the repeatability of the results. The frequency response function (FRF) was obtained by exciting the beam at six predefined locations distributed along its length with a spacing of 4 cm. These measurement points were selected to minimize the influence of nodal positions and provide reliable identification of the vibration characteristics.

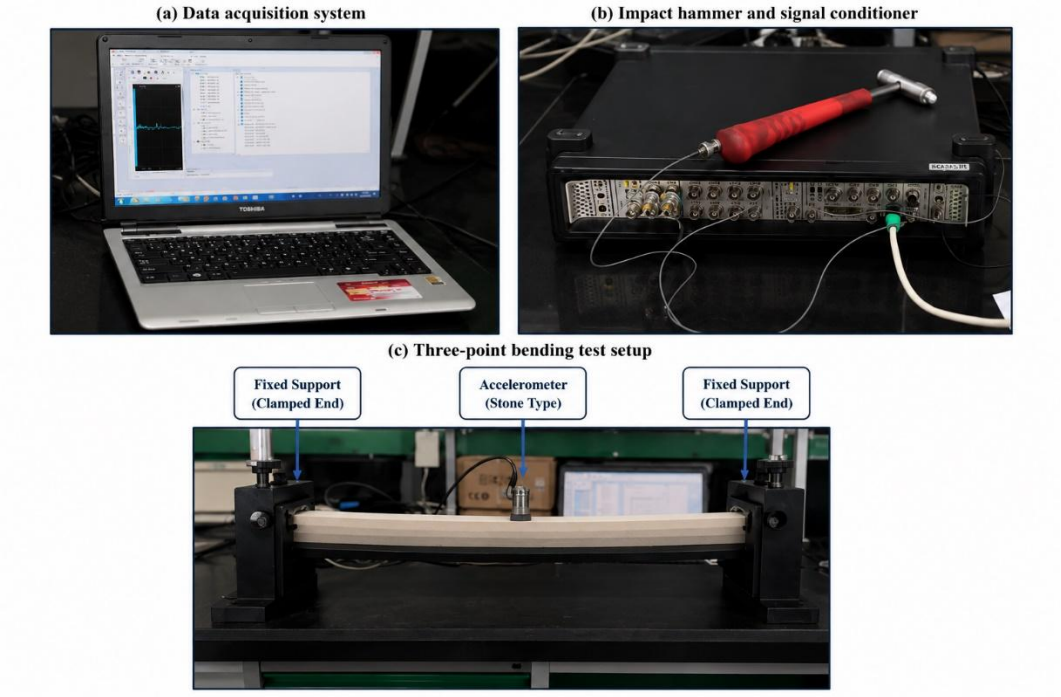


Figure 11. Experimental setup for modal testing of the FGH beam

5. Results and Discussions

Figure 12 illustrates the frequency response function (FRF) obtained from the experimental modal analysis, where distinct resonance peaks associated with the vibration characteristics of the hyperelastic beam are observed. Each peak corresponds to a resonant condition in which the beam exhibits maximum dynamic amplification under impact excitation, representing a specific vibration mode. The locations of these resonance peaks were used to determine the experimental natural frequencies of the fabricated specimen. The measured values for the first and second modes were 22.5 Hz and 56.8 Hz, respectively. These experimental results were subsequently used as reference values to assess the accuracy and reliability of the numerical predictions obtained from the FEM and MCM formulations.

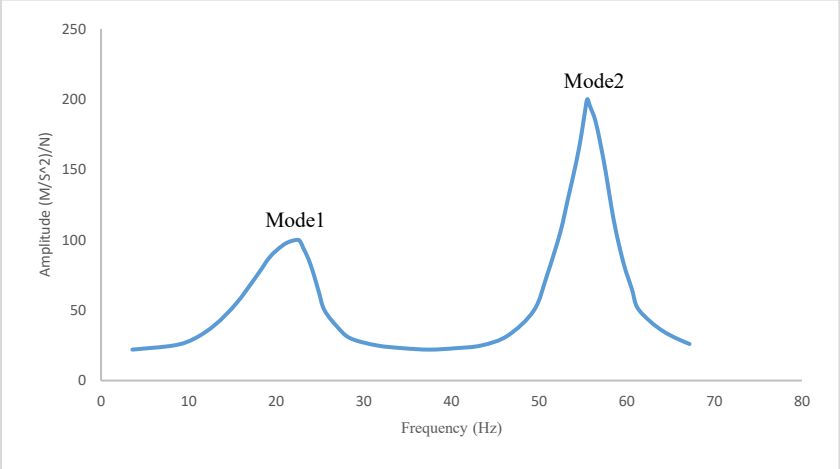


Figure 12. Frequency response of the hyperelastic beam Amplitude at Modes 1 and 2.

The first two natural frequencies obtained from the MCM and FEM approaches are compared with the experimental results in Table 3. A close correlation is observed between the numerical predictions and the measured frequencies, demonstrating the capability of both computational approaches to accurately capture the dynamic response of the functionally graded hyperelastic beam. The MCM predicts the first and second natural frequencies as 21.01 Hz and 54.80 Hz, respectively, while the corresponding FEM results are 21.476 Hz and 55.494 Hz. These values are in good agreement with the experimental measurements of 22.50 Hz and 56.80 Hz, respectively. The small differences between the numerical and experimental results can be attributed to unavoidable variations in material properties, manufacturing imperfections, and simplifications introduced in the numerical boundary conditions.

Vibrational Frequency	Experimental	FEM	MCM	Error FEM (%)	Error MCM (%)
Mode1	22.5	21.476	21.01	4.55	6.62
Mode2	56.8	55.494	54.80	2.30	3.52

Table 3. Free vibration results of the hyperelastic beam

Figure 13 compares the vibration mode shapes predicted by the MCM and FEM approaches in the X–Y plane. Both numerical methods demonstrate a strong correlation in the predicted deformation patterns for the first three vibration modes. The first mode exhibits a single half-wave configuration, whereas the second and third modes present two and three half-wave patterns, respectively. The identical mode shapes and similar deformation distributions obtained from both approaches indicate that the proposed MCM formulation can accurately reproduce the dynamic behavior of the functionally graded hyperelastic beam. This close agreement with the FEM results further verifies the capability of the developed meshless method for analyzing nonlinear vibration problems in hyperelastic structures.

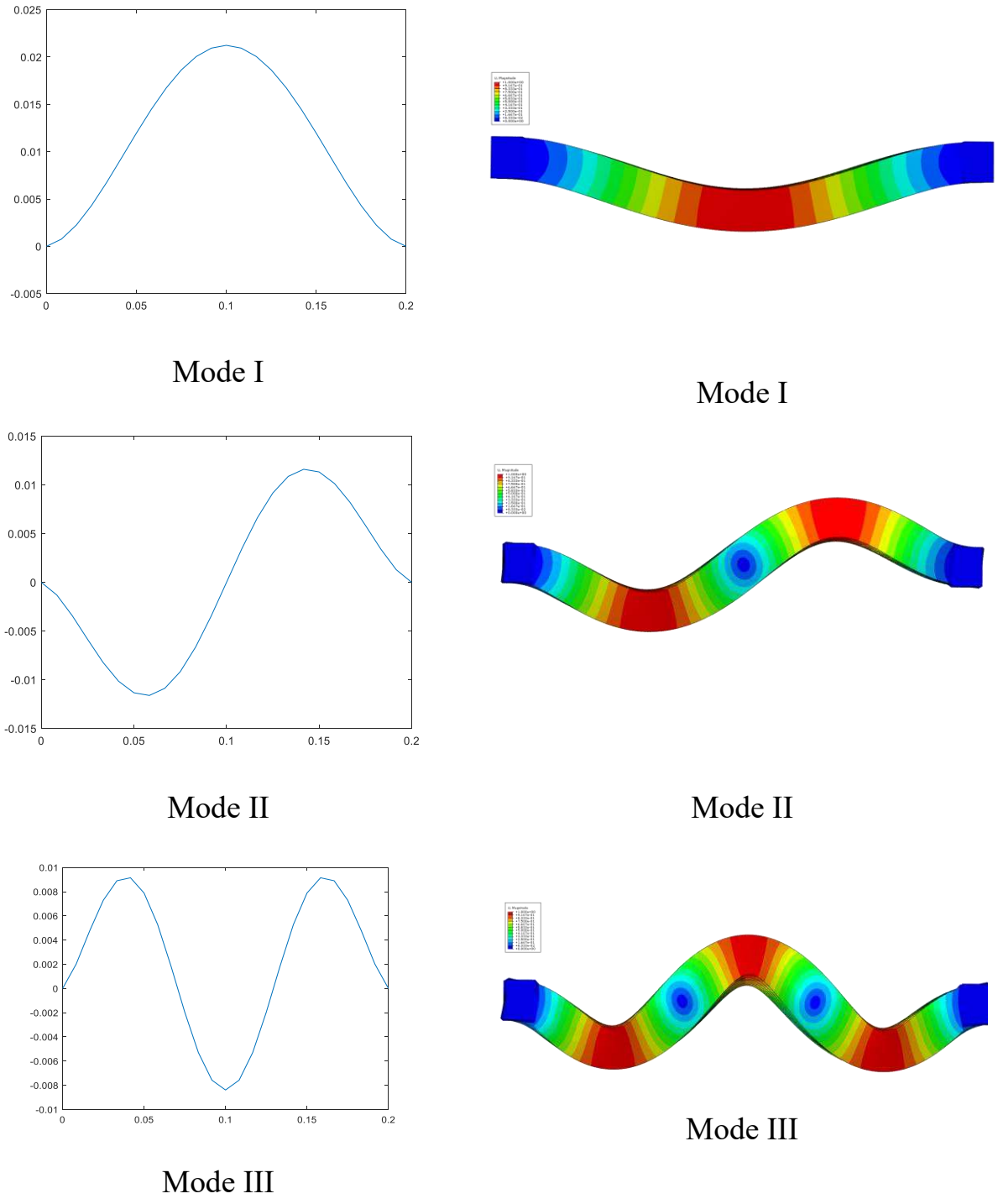


Figure 13. Mode shapes of the FGH beam: (a) MCM and (b) FEM.

6. Parametric study

The free vibration response of the functionally graded hyperelastic (FGH) beam is governed by the interaction between its geometric configuration and material characteristics. In this parametric investigation, the effects of major design variables, including cross-sectional dimensions, beam length, number of graded layers, and Neo-Hookean material parameters, are systematically evaluated. Changes in these variables alter the effective stiffness distribution and dynamic behavior of the beam, resulting in variations in the predicted natural frequencies. The contribution

of each parameter to the vibration characteristics of the FGH beam is discussed in the following subsections.

6.1. Effect of the Number of FGM Layers

Figure 14 presents the effect of the number of functionally graded layers on the first three natural frequencies of the FGH beam. The reference model has a square cross-section of (20 × 20) mm, a length of 250 mm, a Neo-Hookean material parameter of C_{10}=0.8 MPa, a density of 1100kg/m^3, and fixed–fixed boundary conditions. During this parametric study, only the number of graded layers is varied, while all other geometric and material properties are kept constant.
The results show that increasing the number of graded layers from one to eight has only a marginal influence on the natural frequencies. The first natural frequency increases from 24.41 Hz to 24.435 Hz, while the second and third natural frequencies increase from 63.168 Hz to 64.020 Hz and from 115.36 Hz to 115.41 Hz, respectively. This limited variation is attributed to the fact that the overall mass and global stiffness of the beam remain nearly unchanged as the number of layers increases. Consequently, the dynamic response of the beam is almost identical for all layer configurations. The small differences in the predicted natural frequencies arise primarily from the cohesive interfaces between adjacent layers, which introduce slight changes in the effective stiffness of the multilayer beam.

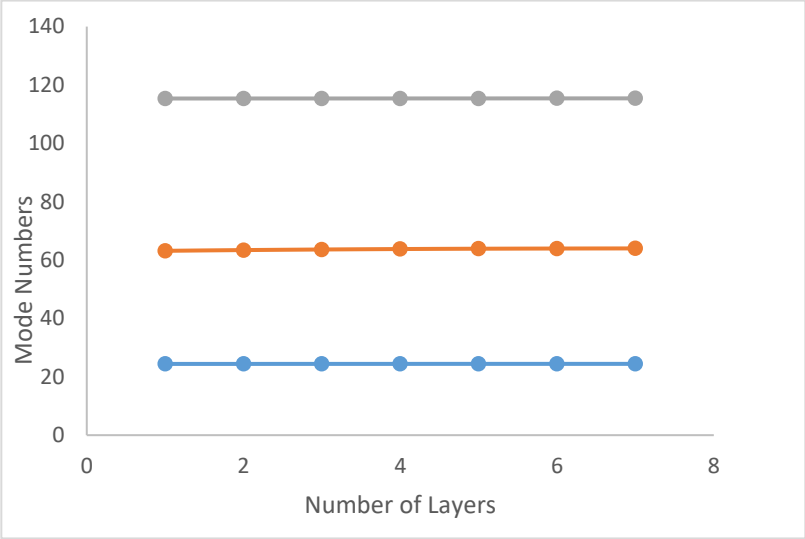


Figure. 14. Effect of the number of FGM layers on natural frequencies.

6.2. Effect of Beam Length

Figure 15 illustrates the effect of beam length on the first three natural frequencies of the FGH beam. The reference model consists of a six-layer beam with a square cross-section of (20 x 20) mm, a Neo-Hookean material parameter of (C_{10}=0.8) MPa, a density of (1100, kg/m^3), and fixed–fixed boundary conditions. During this investigation, only the beam length is varied, while all other geometric and material parameters remain unchanged. As shown in Figure 15, increasing the beam length from 100 mm to 400 mm causes a significant reduction in the natural frequencies of all vibration modes. The first natural frequency decreases from 43.10 Hz to 11.40 Hz, whereas the second and third natural frequencies decrease from 111.60 Hz to 29.20 Hz and from 203.60 Hz to 53.10 Hz, respectively. This behavior is attributed to the reduction in the beam's bending stiffness as the span increases. Although the mass also increases with beam length, the reduction in stiffness

is much more pronounced, leading to a lower stiffness-to-mass ratio and consequently lower natural frequencies. Furthermore, increasing the slenderness ratio (L/H) enhances the structural flexibility, making longer beams more susceptible to deformation and vibration. These results indicate that beam length is one of the most influential geometric parameters affecting the dynamic behavior of the FGH beam and should be carefully considered during structural design to achieve the desired vibration performance.

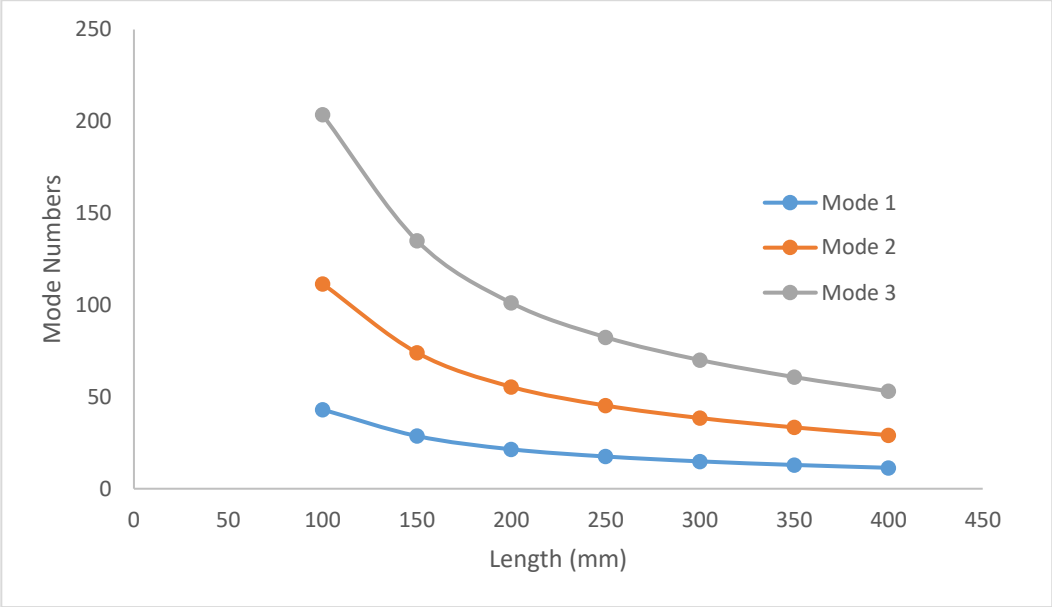


Figure. 15. Effect of beam length on natural frequencies.

6.3. Effect of Cross-Sectional Dimensions

Figure 16 illustrates the effect of the beam cross-sectional dimensions on the first three natural frequencies of the FGH beam. The reference model consists of a six-layer beam with a length of 250 mm, a Neo-Hookean material parameter of C_{10}=0.8 MPa, a density of 1100, kg/m^3, and fixed–fixed boundary conditions. During this parametric study, the beam width and height are increased simultaneously from (10 x 10) mm to (40 x 40) mm, while all other parameters remain unchanged. Enlarging the beam cross-section leads to a substantial increase in the natural frequencies of all vibration modes. The first natural frequency increases from 10.82 Hz for the (10 x10) mm beam to 43.15 Hz for the (40 x 40) mm beam, while the second and third natural frequencies increase from 27.95 Hz to 111.50 Hz and from 50.90 Hz to 203.20 Hz, respectively. This trend is primarily attributed to the significant increase in bending stiffness associated with the larger second moment of area. Although the beam mass also increases with the cross-sectional dimensions, the stiffness increases at a much higher rate, resulting in a larger stiffness-to-mass ratio and consequently higher natural frequencies. The increase is more pronounced for smaller cross-sections, whereas the rate of change gradually decreases as the beam dimensions become larger. These findings demonstrate that the beam cross-section is one of the most influential geometric parameters governing the dynamic behavior of the FGH beam and provides an effective design variable for tailoring its vibration characteristics.

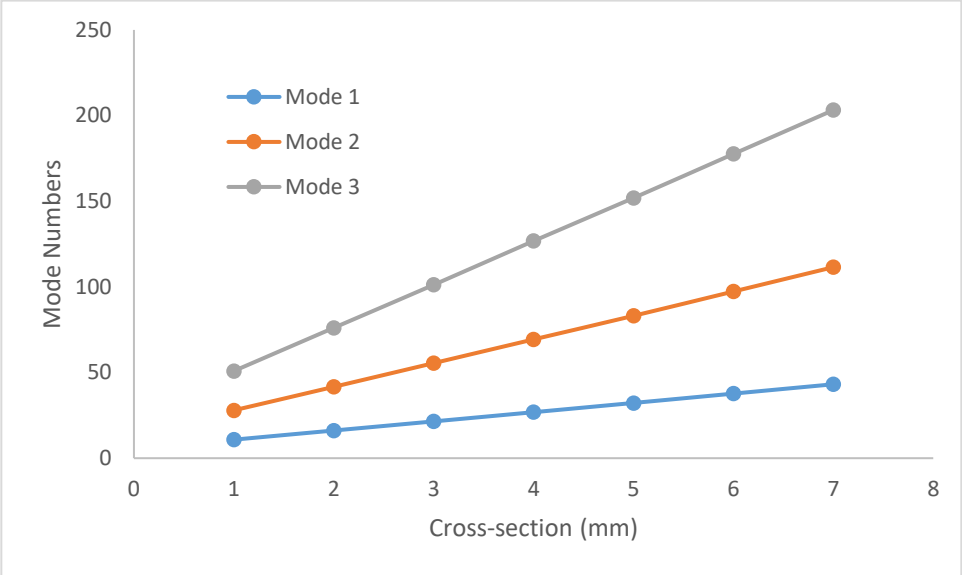


Figure. 16. Effect of cross-sectional dimensions on natural frequencies.

6.3. Effect of the Neo-Hookean Material Parameter

Figure 17 presents the effect of the Neo-Hookean material parameter C_{10} on the first three natural frequencies of the FGH beam. The reference model consists of a six-layer beam with a square cross-section of (20 x 20) mm, a length of 250 mm, a density of (1100kg/m^3), and fixed–fixed boundary conditions. During this parametric investigation, only the Neo-Hookean material parameter is varied from 40% to 140% of its reference value, while all other geometric and material properties are kept constant. The results demonstrate that increasing C_{10} leads to a significant increase in the natural frequencies of all vibration modes. The first natural frequency rises from 13.70 Hz at 40% of the reference value to 25.35 Hz at 140%, while the second and third natural frequencies increase from 35.40 Hz to 65.40 Hz and from 64.60 Hz to 119.30 Hz, respectively. This trend is attributed to the increase in the elastic stiffness of the hyperelastic material with increasing C_{10}. Since the beam geometry and density remain unchanged, the increase in stiffness results in a higher stiffness to mass ratio, which directly increases the natural frequencies. Moreover, the response of all three vibration modes follows an approximately linear trend over the investigated range, indicating a strong dependence of the dynamic characteristics on the Neo-Hookean material parameter. These findings demonstrate that (C_{10}) is a key material parameter for tuning the vibration performance of functionally graded hyperelastic beams and should be carefully considered during the design process.

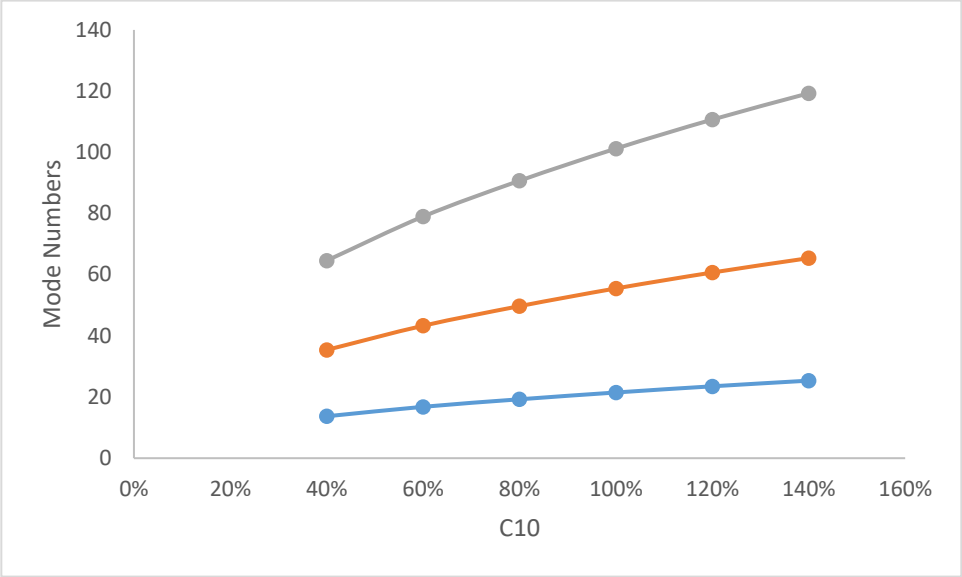


Figure. 17. Effect of the Neo-Hookean parameter on natural frequencies.

Table 4 summarizes the results of the parametric investigation performed to evaluate the effects of the number of FGM layers, beam length, cross-sectional dimensions, and Neo-Hookean material parameter on the first three natural frequencies of the functionally graded hyperelastic beam. The results demonstrate that the dynamic response of the beam is strongly influenced by both geometric and material parameters. Increasing the number of graded layers leads to a gradual increase in natural frequencies due to the smoother distribution of material properties and improved stiffness continuity through the beam thickness. In contrast, increasing the beam length reduces the vibration frequencies because of the reduction in bending rigidity and the increase in structural flexibility. Furthermore, larger cross-sectional dimensions significantly enhance the natural frequencies by increasing the moment of inertia and overall stiffness of the beam. The increase in the Neo-Hookean parameter also results in higher frequencies due to the increased effective stiffness of the hyperelastic material. These results confirm that appropriate control of material gradation and geometric parameters can effectively tailor the vibration characteristics of FGH beams.

Parameter	Value	Mode 1 (Hz)	Mode 2 (Hz)	Mode 3 (Hz)
Effect of the number of FGM layers				
Number of layers	1	20.62	53.28	96.8
	2	20.95	54.1	98.25
	4	21.15	54.62	99.4
	6	21.3	55.02	100.35
	8	21.4	55.28	100.85
Effect of beam length				
Beam length (mm)	L = 100	43.10	111.60	203.60
	L = 200	21.476	55.494	101.21
	L = 300	14.90	38.50	70.10
	L = 400	11.40	29.20	53.10
Effect of cross-sectional dimensions				
Cross-section (mm^2)	10 × 10	10.82	27.95	50.90
	20 × 20	21.476	55.494	101.21
	30 × 30	32.25	83.10	151.90
	40 × 40	43.15	111.50	203.20
Effect of Neo-Hookean constant				
Material constant	40%	13.70	35.40	64.60
	60%	16.80	43.30	79.00
	80%	19.25	49.70	90.70
	100%	21.476	55.494	101.21
	120%	23.50	60.70	110.70
	140%	25.35	65.40	119.30

Table 4. Effects of geometric and material parameters on the first three natural frequencies of the FGH beam.

7. Artificial Neural Networks

7.1. Introduction to ANN Modeling

Artificial Neural Networks (ANNs) have emerged as powerful data-driven tools for predicting the response of complex engineering systems with high accuracy and significantly reduced computational effort. In the present study, a feedforward ANN is developed to predict the first three natural frequencies of the functionally graded hyperelastic (FGH) beam based on its geometric and material parameters. The input variables consist of the beam length (L), cross-sectional dimensions (B × H), Neo-Hookean material parameter C_{10}, and the number of functionally graded layers. The output variables are the first three natural frequencies (Modes 1–3) (table 5). The training dataset was generated from the validated Meshless Collocation Method (MCM) and finite element (FE) simulations through a comprehensive parametric study. The dataset was randomly divided into 70% for training, 15% for validation, and 15% for testing to ensure reliable prediction capability. The ANN architecture comprises four input neurons, a single hidden layer containing ten neurons, and three output neurons corresponding to the first three vibration modes. The network was trained using the Levenberg–Marquardt backpropagation algorithm with a learning rate of 0.001 for 400 epochs. The predictive performance of the proposed model was evaluated using the Mean Squared Error (MSE) and the coefficient of determination (R^2).

Design Variable	Symbol	Range
Input: Beam length	L	10–800 mm
Input: Cross-sectional dimension	B x H	5 × 5 – 100 × 100 mm²
Input: Neo-Hookean parameter	C_{10}	0.1 Mpa – 3 Mpa
Input: Number of FGM layers	N	1–15
Output: First natural frequency	f_1	4–40 Hz
Output: Second natural frequency	f_2	10–140 Hz
Output: Third natural frequency	f_3	20–400 Hz

Table 5. Design variables of the investigated FGM hyperelastic Beam structure.

7.2. Neural Network Implementation

The performance of the developed ANN model was evaluated using the mean squared error (MSE) and coefficient of determination (R^2), and the predicted natural frequencies were compared with the numerical results obtained from the validated MCM/FEM models. Figure 18 illustrates the training, validation, and testing performance of the ANN during 400 training epochs. The error decreases rapidly during the initial training stages and gradually converges, indicating stable learning behavior. The close agreement between the training, validation, and testing curves demonstrates that the proposed network achieves good generalization capability without significant overfitting.

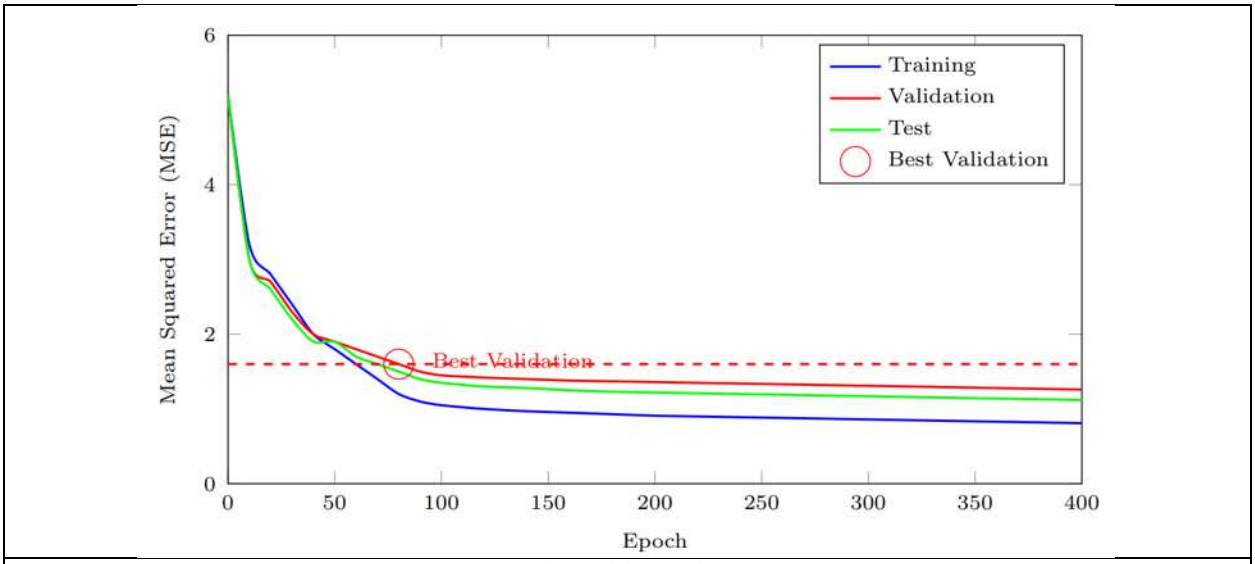


Figure 18. ANN training, validation, and testing performance.

Figure 19 presents the regression analysis between the ANN-predicted and reference natural frequencies for the training, validation, testing, and overall datasets. The data points are closely distributed around the ideal regression line, confirming the ability of the ANN model to capture the nonlinear relationship between the input parameters (beam length, cross-sectional dimensions, Neo-Hookean parameter, and number of FGM layers and the output responses (first three natural frequencies). The obtained (R^2) values demonstrate the high prediction accuracy of the proposed model.

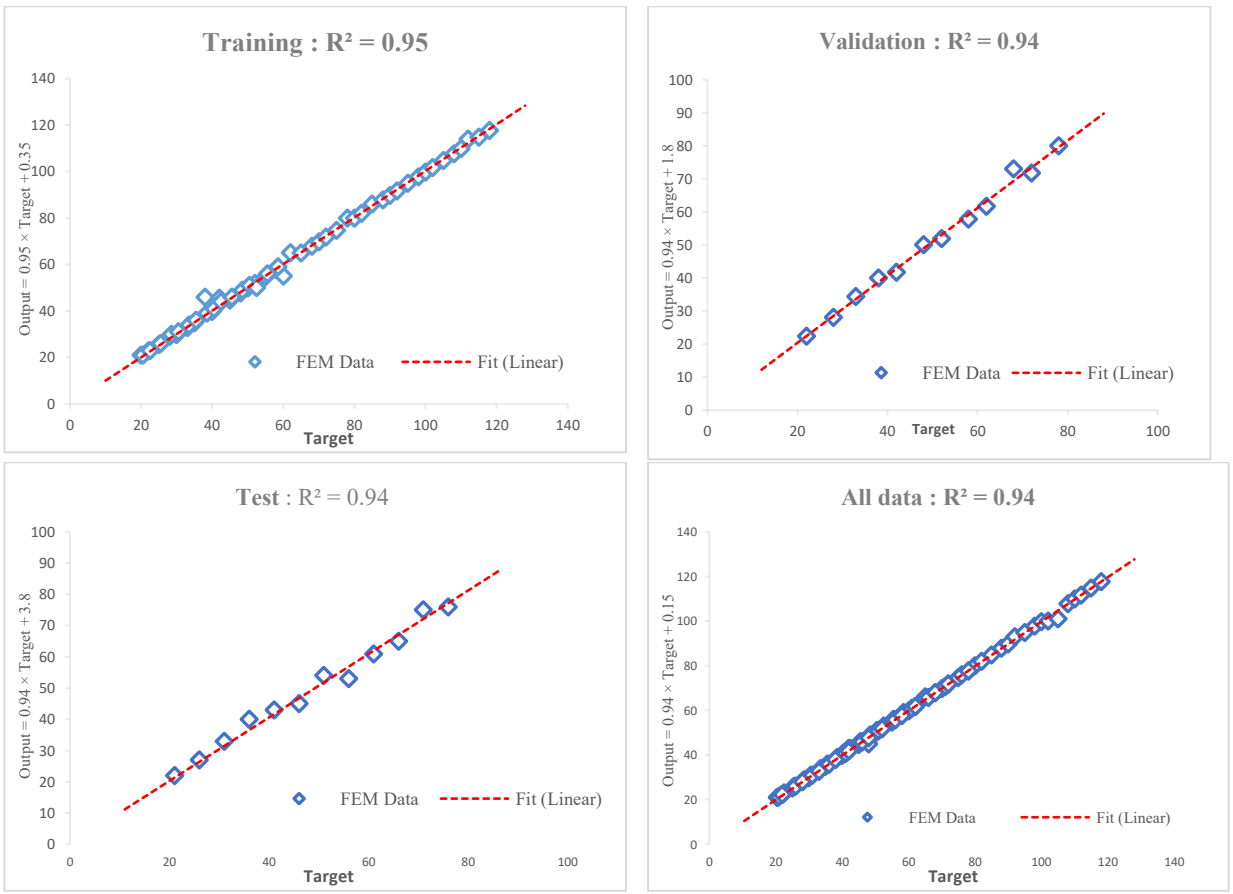


Figure 19. ANN regression plots for (a) training, (b) validation, (c) testing, and (d) all datasets.

To further verify the reliability of the ANN approach, the predicted frequencies were compared with the corresponding FEM results for selected beam configurations, as presented in Table 6. The comparison shows excellent agreement between ANN predictions and numerical simulations, with small prediction errors for all vibration modes. These results confirm that the developed ANN model can provide an efficient alternative to repeated finite element simulations, particularly for parametric studies and vibration-based design optimization of functionally graded hyperelastic beams.

Method	L (mm)	Cross-section (mm²)	Number of Layers	C10(%)	Mode 1 (Hz)	Error (%)	Mode 2 (Hz)	Error (%)	Mode 3 (Hz)	Error (%)
FEM	200	20 × 20	6	100	21.476	–	55.494	–	101.21	–
ANN	200	20 × 20	6	100	21.242	1%	55.121	1.5%	100.020	1.1%

Table 6. Comparison of ANN and FEM predictions for the natural frequencies of the FGH beam.

8. Conclusion

This study presented a comprehensive numerical and data-driven investigation of the free vibration behavior of functionally graded hyperelastic (FGH) beams. The governing equations were formulated based on Timoshenko beam theory and the Neo-Hookean hyperelastic constitutive model and solved using the Meshless Collocation Method (MCM). The proposed formulation was validated through finite element (FE) simulations performed in Abaqus and experimental modal testing. The numerical predictions obtained using the MCM exhibited excellent agreement with the FE results, while the maximum discrepancy between the MCM predictions and the experimental natural frequencies remained below 6.63%, confirming the accuracy and reliability of the proposed meshless formulation for analyzing the dynamic behavior of multilayer hyperelastic beams.

A comprehensive parametric study was performed to examine the effects of the number of functionally graded layers, beam length, cross-sectional dimensions, and the Neo-Hookean material parameter C_{10}on the natural frequencies. The results demonstrated that increasing the number of graded layers slightly enhances the vibration characteristics owing to the smoother through-thickness stiffness distribution. In contrast, increasing the beam length significantly decreases the natural frequencies because of the reduction in global flexural stiffness. Conversely, larger cross-sectional dimensions and higher C_{10}values increase the structural stiffness, leading to higher natural frequencies. Among the investigated parameters, the beam length and cross-sectional dimensions were found to have the greatest influence on the dynamic response of the FGH beam.

Furthermore, a multilayer perceptron artificial neural network (ANN) was developed using the validated numerical dataset generated by the MCM and FE analyses. The trained ANN accurately predicted the first three natural frequencies with high precision while significantly reducing the computational cost associated with repeated numerical simulations. Consequently, the proposed ANN provides an efficient surrogate model for rapid vibration prediction, parametric analyses, sensitivity studies, and preliminary design optimization of functionally graded hyperelastic beam structures.

Funding: No funding was received for conducting this study.

References

1. Shakeriaski, F., et al., *The nonlinear thermo-hyperelasticity wave propagation analysis of near-incompressible functionally graded medium under mechanical and thermal loadings.* Archive of Applied Mechanics, 2021. **91**(7): p. 3075.
2. Chen, J., et al., *The effect of hyperelasticity and nonlinearity on the dynamic behaviors of hyperelastic functionally graded beams on nonlinear elastic foundation.* International Journal of Structural Stability and Dynamics, 2025. **25**(09): p. 2550096.
3. Forsat, M., *Investigating nonlinear vibrations of higher-order hyper-elastic beams using the Hamiltonian method.* Acta Mechanica, 2020. **231**(1): p. 125.
4. Saeidiha, M., H. Ahmadi, and A. Jalali, *Nonlinear vibrations analysis of hyperelastic cylindrical shells utilizing the method of multiple scales.* International Journal of Structural Stability and Dynamics, 2024. **24**(17): p. 2450209.
5. Foroutan, K., H. Ahmadi, and S. Karimi, *Nonlinear vibration and resonance analysis of a rectangular hyperelastic membrane surrounded by nonlinear elastic foundation.* Mechanics Based Design of Structures and Machines, 2024. **52**(7): p. 4616–4641.
6. Jebellat, E. and I. Jebellat, *Stress analysis of functionally graded hyperelastic variable thickness rotating annular thin disk: A semi-analytic approach.* arXiv preprint arXiv:2404.11365, 2024.
7. Hamad, A.G., et al., *Large Deformation Analysis of Rotating Variable-Thickness Homogeneous and FGM Hyperelastic Disks using PINNs.* International Journal of Structural Stability and Dynamics, 2025: p. 2750139.
8. Mirparizi, M., S.M. Razavinasab, and M. Mohammadian, *Interference of Thermal and Mechanical Waves in a Functionally Graded Hyperelastic Model Exhibits both Temperature and Coordinate Dependencies.* Journal of Applied and Computational Mechanics, 2026. **12**(1): p. 40–50.
9. Maslak, A.T. and A. Alibeigloo, *Three-dimensional piezo-viscoelastic behavior of FGM cylindrical panel with piezoelectric layers under electro-mechanical loads.* Archives of Civil and Mechanical Engineering, 2023. **24**(1): p. 10.
10. Kaveh, A., et al., *Vibrational response of a sandwich microplate considering the impact of flexoelectricity and based on a novel porous-FGM formulation.* Mechanics Based Design of Structures and Machines, 2024. **52**(11): p. 9122–9143.
11. Karami Mohammadi, A. and S. Danaee Barforooshi, *Free vibration of a hyper-elastic microbeam using a new "augmented Biderman model".* Journal of Theoretical and Applied Mechanics, 2019. **57**.
12. Khaniki, H.B., et al., *Nonlinear continuum mechanics of thick hyperelastic sandwich beams using various shear deformable beam theories.* Continuum Mechanics and Thermodynamics, 2022. **34**(3): p. 781–827.
13. Khaniki, H.B., et al., *Internal resonance and bending analysis of thick visco-hyper-elastic arches.* Continuum Mechanics and Thermodynamics, 2022: p. 1–44.
14. Azarniya, O. and G.H. Rahimi, *Numerical and experimental analysis of free vibrations and static bending of a sandwich beam with a hyperelastic core.* Mechanics Based Design of Structures and Machines, 2022: p. 1–23.
15. Zolfagharian, A., et al., *3D-printed programmable mechanical metamaterials for vibration isolation and buckling control.* Sustainability, 2022. **14**(11): p. 6831.
16. Chen, M. and L. Ling, *Extrinsic meshless collocation methods for PDEs on manifolds.* SIAM Journal on Numerical Analysis, 2020. **58**(2): p. 988–1007.
17. Zhang, Y., et al., *A novel local meshless collocation method with partial upwind scheme for solving convection-dominated diffusion problems.* Engineering with Computers, 2025. **41**(1): p. 353–368.
18. Hosseini, S., G. Rahimi, and Y. Anani, *A meshless collocation method based on radial basis functions for free and forced vibration analysis of functionally graded plates using FSDT.* Engineering Analysis with Boundary Elements, 2021. **125**: p. 168–177.
19. Li, M., et al., *An efficient localized meshless collocation method for the two-dimensional Burgers-type equation arising in fluid turbulent flows.* Engineering Analysis with Boundary Elements, 2022. **144**: p. 44–54.

20. Zhang, S., *Meshless symplectic and multi-symplectic local RBF collocation methods for Hamiltonian PDEs.* Journal of Scientific Computing, 2021. **88**(3): p. 90.
21. Abbaszadeh, M., H. Pourbashash, and M. Khaksar-e Oshagh, *The local meshless collocation method for solving 2D fractional Klein-Kramers dynamics equation on irregular domains.* International Journal of Numerical Methods for Heat & Fluid Flow, 2022. **32**(1): p. 41–61.
22. Patel, V.G. and N.V. Rachchh, *Meshless method–review on recent developments.* Materials today: proceedings, 2020. **26**: p. 1598–1603.
23. Radmanesh, M. and M. Ebadi, *A local mesh-less collocation method for solving a class of time-dependent fractional integral equations: 2D fractional evolution equation.* Engineering analysis with boundary elements, 2020. **113**: p. 372–381.
24. Siłka, J., M. Wieczorek, and M. Woźniak, *Recurrent neural network model for high-speed train vibration prediction from time series.* Neural Computing and Applications, 2022. **34**(16): p. 13305–13318.
25. Fissha, Y., et al., *Application of Bayesian neural network (BNN) for the prediction of blast-induced ground vibration.* Applied sciences, 2023. **13**(5): p. 3128.
26. Lawal, A.I. and M.A. Idris, *An artificial neural network-based mathematical model for the prediction of blast-induced ground vibrations.* International Journal of Environmental Studies, 2020. **77**(2): p. 318–334.
27. Lawal, A.I., *An artificial neural network-based mathematical model for the prediction of blast-induced ground vibration in granite quarries in Ibadan, Oyo State, Nigeria.* Scientific African, 2020. **8**: p. e00413.
28. Liang, R., et al., *An efficient model for predicting the train-induced ground-borne vibration and uncertainty quantification based on Bayesian neural network.* Journal of Sound and Vibration, 2021. **495**: p. 115908.
29. Zollanvari, A., et al., *Transformer fault prognosis using deep recurrent neural network over vibration signals.* IEEE Transactions on Instrumentation and Measurement, 2020. **70**: p. 1–11.
30. Shang, Y., et al., *A novel artificial intelligence approach to predict blast-induced ground vibration in open-pit mines based on the firefly algorithm and artificial neural network.* Natural Resources Research, 2020. **29**(2): p. 723–737.
31. Tang, H., et al., *A transfer learning-physics informed neural network (TL-PINN) for vortex-induced vibration.* Ocean Engineering, 2022. **266**: p. 113101.
32. Jamil, M., et al., *Neural network predictive control of vibrations in tall structure: An experimental controlled vision.* Computers & Electrical Engineering, 2021. **89**: p. 106940.
33. Nguyen, H. and X.-N. Bui, *A novel hunger games search optimization-based artificial neural network for predicting ground vibration intensity induced by mine blasting.* Natural Resources Research, 2021. **30**(5): p. 3865–3880.
34. Alijani, F. and M. Amabili, *Non-linear vibrations of shells: A literature review from 2003 to 2013.* International journal of non-linear mechanics, 2014. **58**: p. 233–257.
35. Khaniki, H.B., et al., *Hyperelastic structures: A review on the mechanics and biomechanics.* International Journal of Non-Linear Mechanics, 2022: p. 104275.
36. Faghihi, S., et al., *Graphene oxide/poly (acrylic acid)/gelatin nanocomposite hydrogel: Experimental and numerical validation of hyperelastic model.* Materials Science and Engineering: C, 2014. **38**: p. 299–305.
37. Hu, D.a. and Z. Sun, *The meshless local petrov-galerkin method for large deformation analysis of hyperelastic materials.* International Scholarly Research Notices, 2011. **2011**.
38. Fouaidi, M., M. Jamal, and N. Belouaggadia, *Nonlinear bending analysis of functionally graded porous beams using the multiquadric radial basis functions and a Taylor series-based continuation procedure.* Composite Structures, 2020. **252**: p. 112593.
39. Fouaidi, M., et al., *Multiquadric radial basis function approximation method and asymptotic numerical method for nonlinear and linear static analysis of single-walled carbon nanotubes.* Engineering Analysis With Boundary Elements, 2020. **115**: p. 40–51.
40. Chen, W., L. Wang, and H. Dai, *Nonlinear free vibration of hyperelastic beams based on neo-Hookean model.* International Journal of Structural Stability and Dynamics, 2020. **20**(01): p. 2050015.

41. Liu, F., Q. Wu, and Y. Cheng, *A meshless method based on the nonsingular weight functions for elastoplastic large deformation problems.* International Journal of Applied Mechanics, 2019. **11**(01): p. 1950006.
42. Liu, F. and Y. Cheng, *The improved element-free Galerkin method based on the nonsingular weight functions for inhomogeneous swelling of polymer gels.* International Journal of Applied Mechanics, 2018. **10**(04): p. 1850047.
43. Huang, J., et al., *Static, free vibration, and buckling analyses of laminated composite plates via an isogeometric meshfree collocation approach.* Composite Structures, 2022. **285**: p. 115011.
44. Hosseini, S. and G. Rahimi, *Nonlinear bending analysis of hyperelastic plates using FSDT and meshless collocation method based on radial basis function.* International Journal of Applied Mechanics, 2021. **13**(01): p. 2150007.